Journal of Fluids and Structures (1997) **11,** 745–766

SYMMETRICALLY OSCILLATING VISCOUS FLOW OVER AN ELLIPTIC CYLINDER

H. M. Badr

Mechanical Engineering Department, King Fahd University of Petroleum and Minerals Dhahran 31261, Saudi Arabia

AND

S. Kocabiyik

Department of Applied Mathematics, University of Manitoba Winnipeg, Manitoba, R3T 2N2, Canada

(Received 12 April 1996 and in revised form 9 June 1997)

The paper deals with the problem of two-dimensional oscillating viscous flow past an elliptic cylinder. The flow is considered incompressible and two-dimensional, and the free-stream oscillations are harmonic. These oscillations are only allowed in the magnitude of the free-stream velocity, which is always parallel to one of the elliptic section axes. The resulting flow field is symmetrical about either the major or minor axis of the ellipse. The parameters involved are the cylinder axis ratio, Reynolds number and the oscillation frequency. The major-minor axis ratio of the elliptic cylinder ranges between 0·5 and 0·8, the Reynolds number ranges between 500 and 10^3, and the frequency parameter ranges between $\pi/4$ and $\pi/2$. Present calculations are performed within the range of sufficiently large oscillation amplitude to induce separation. The time variation of the flow field is presented in the form of streamline patterns as well as the surface pressure distribution. The time variation of the drag coefficients is also presented and compared with the inviscid flow solution. The results show that the force coefficient predicted for the case of viscous flow approaches that of potential flow as the Reynolds number and frequency increase.

1. INTRODUCTION

Originally, interest in oscillatory flow of a viscous fluid past cylinders and spheres centred on application of the results to the design of vertical piles subjected to ocean waves. However, more recent interest covers a wider area and includes the prediction of wave-induced forces on ocean structures of all shapes such as habitats, oil-storage tanks, space-frame structures in fixed or floating platforms, etc. In this paper we study two-dimensional symmetric flow generated by an elliptic cylinder placed in an oscillatory flow environment of infinite extent. The cylinder with major and minor axes lengths $2a$ and $2b$, respectively, is at rest in a flow whose oscillations are represented by $U \cos \omega t^*$. Here t^* is the time and ω is the frequency of oscillation. Translational oscillations are allowed only about an axis which coincides with either the major or minor axis of the ellipse. The motion is assumed to be governed by the Navier-Stokes equations for an incompressible fluid and the flow is laminar. We shall take axes fixed with the origin at the centre of the cylinder and

0889-9746/97/070745 + 22 $25.00/fl970100

regard the fluid as oscillating. The three basic parameters involved in this problem are the major-minor axis ratio, b/a, the Reynolds number defined as $\mathrm{Re} = U(2a)/\nu$, where ν is the fluid kinematic viscosity, and the reduced frequency α, defined as $\alpha = a\omega/U$. This reduced frequency is related to the Keulegan-Carpenter number, KC, by $KC = \pi/\alpha$.

There are numerous theoretical, numerical and experimental investigations on translational oscillatory flows about cylinders of circular cross-section. The most recent studies on translational oscillatory flows around a circular cylinder have been made by Zhang & Dalton (1993), Badr *et al.* (1995a) and Badr *et al.* (1995b). In the work by Zhang & Dalton (1993), numerical solutions were obtained for viscosity-dominated oscillating flow past a rigid cylinder considering sinusoidal and nonsinusiodal oscillations. A very good agreement was found between the calculated and experimental force coefficients in the case of sinusoidal oscillations. Badr *et al.* (1995b) conducted a numerical study on the transient flow field caused by a circular cylinder placed in an unbounded viscous fluid oscillating in a direction normal to the cylinder axis. Numerical solutions were obtained for large values of time for both moderate and high Reynolds numbers. The accuracy of the numerical scheme was verified by comparing the results with those obtained from the analytical solution of Badr *et al.* (1995a) at small times. A useful review of oscillating flows of this type is provided by Riley (1967) and Sarpkaya(1979); see also Badr *et al.* (1995b) and Nguyen & Kocabiyik (1996).

There has been some interest in carrying out the calculations for elliptic cylinders, since these include the problems of the circular cylinder and flat plate as limiting cases. For oscillatory flows about elliptic cylinders, references may be made only to the works of Davidson & Riley (1972), Taneda (1977), Badr (1994a, b) and Riley & Wybrow (1995). Davidson & Riley (1972) have studied the periodic, but not purely harmonic, transverse motion of elliptic cylinders both theoretically and experimentally. In their work a complete numerical integration of boundary-layer equations for a class of elliptic cylinders has been performed to trace the origin of the time-averaged, thin jet-like flow which emerges along the axis of oscillation. Davidson & Riley also visualized and made measurements of these jet-like flows. Taneda (1977) visualized the streamline patterns in the case of an elliptic cylinder oscillating in a quiescent fluid for a cylinder axis ratio 0·5 at 30° incidence. The experiment was carried out for Reynolds numbers of 48 and 144 only.

Badr (1994a) considered oscillating inviscid flow over elliptic cylinders. In this work, analytical expressions are given for the drag coefficient, the lift coefficient, and their variation with time. Similar analytical expressions are also given in Badr's work for the special cases of circular cylinders and inclined flat plates in oscillating inviscid flows. Badr (1994b) was the first to study the problem of oscillating viscous flow over an elliptic cylinder for an angle of attack $\lambda = 30^\circ$ or 60°. In his work, oscillations were harmonic and the flow direction was normal to the cylinder axis. Badr (1994b) carried out a very careful numerical study to calculate the flow properties for a cylinder axis ratio of 0·6 when the Reynolds number ranges between 10^2 and 10^3. His calculations were performed within the range of sufficiently large oscillation amplitude to induce separation. In Badr's work more emphasis is placed on the governing equations and the accuracy of the method of solution, with applications to a limited number of cases. Riley & Wybrow (1995) considered the fluid motion induced when an elliptic cylinder performs small-amplitude torsional oscillations about an axis parallel to a generator which passes through either the centre or a point on the major or minor axis of the ellipse. Their work focuses on the acoustic streaming, or time-averaged flow, and several unusual and unexpected features of steady streaming were confirmed by experiments.

This paper aims to study the problem of symmetrically oscillating viscous flow over an elliptic cylinder for the two cases when the axis of the translational oscillation coincides with either the major or minor axis of the ellipse. Particular interest is focused on the effect of Reynolds number and oscillation frequency on the deviation from the analytical solution of the force coefficients for the inviscid flow case. The details of the vortex structure (including vortex formation and decay) and its relation to the accelerating and decelerating flow periods are also investigated for the two flow configurations. The problem is solved for Reynolds number ranging from 200 to 10^3, and for two values of the reduced frequency ($\pi/4$ and $\pi/2$) when the major-minor axis ratio ranges between 0·5 and 0·8. Results obtained for surface pressure distribution and the time variation of the in-line and transverse force coefficients are compared with an analytical solution of the inviscid flow problem. The results of this study are of theoretical and practical importance, since it adds to the knowledge of the mechanism of vortex formation and decay and is directly related to several engineering applications.

2. GOVERNING EQUATIONS AND METHOD OF SOLUTION

At time $t = 0$, the viscous incompressible fluid surrounding an infinitely long elliptic cylinder suddenly starts to oscillate along an axis of symmetry. The free stream, far away from the cylinder surface, exhibits harmonic oscillations in the horizontal direction. The direction of fluid motion is always normal to the cylinder axis. Attention is focused upon two particular situations, both of which involve an elliptic cylinder of major and minor axes $2a$ and $2b$. In the first, the x and y coordinates are along the major and minor axes whereas in the second, the x and y coordinates are along the minor and major axes. Using the elliptic coordinates (ξ, η), the appropriate transformation is

$$x = c \cosh \xi \cos \eta, \qquad y = c \sinh \xi \sin \eta$$

where $c = c^*/a = \sec \xi_0$. Here c^* is the dimensional focal distance and $\xi_0 = \tanh^{-1}(b/a)$ defines the surface of the cylinder. The motion is two-dimensional and may be described in terms of the usual two simultaneous equations satisfied by the stream function and the scalar vorticity. If ψ^* and ζ^* are the dimensional stream function and vorticity associated with the motion, we introduce the dimensionless functions ψ and ζ defined by the equations,

$$\psi^* = Ua\psi \quad \text{and} \quad \zeta^* = -U\zeta/a$$

The dimensionless velocity components (v_ξ, v_η) in the directions of increase of ξ and η are given by

$$v_\xi = \frac{1}{H^{1/2}} \frac{\partial \psi}{\partial \eta'}, \quad v_\eta = \frac{1}{H^{1/2}} \frac{\partial \psi}{\partial \xi} \tag{1}$$

and the function ξ is defined by

$$\zeta = \frac{1}{H} \left[\frac{\partial}{\partial \eta} (H^{1/2} v_\xi) - \frac{\partial}{\partial \xi} (H^{1/2} v_\eta) \right] \tag{2}$$

Here ψ and ζ satisfy the unsteady Navier-Stokes equations,

$$H \frac{\partial \zeta}{\partial t} = \frac{2}{\mathrm{Re}} \left(\frac{\partial^2 \zeta}{\partial \xi^2} + \frac{\partial^2 \zeta}{\partial \eta^2} \right) + \left(\frac{\partial \psi}{\partial \xi} \frac{\partial \zeta}{\partial \eta} - \frac{\partial \psi}{\partial \eta} \frac{\partial \zeta}{\partial \xi} \right) \tag{3}$$

$$\frac{\partial^2 \psi}{\partial \xi^2} + \frac{\partial^2 \psi}{\partial \eta^2} = H\zeta \tag{4}$$

where t is the dimensionless time defined by $t = Ut^*/a$ and $H = c^2(\cosh 2\xi - \cos 2\eta)/2$.

The boundary conditions are simply the no-slip and impermeability conditions at the solid surface, and the free-stream conditions far away from it which may be stated as

$$\psi = \frac{\partial \psi}{\partial \xi} = 0 \quad \text{when} \quad \xi = \xi_0 \tag{5}$$

$$\frac{\partial \psi}{\partial \xi} \to \frac{c}{2} e^{\xi} \sin(\eta - \lambda) \cos \alpha t, \quad \frac{\partial \psi}{\partial \eta} \to \frac{c}{2} e^{\xi} \cos(\eta - \lambda) \cos \alpha t \quad \text{as } \xi \to \infty \tag{6}$$

Here the flow oscillation enters through the reduced frequency $\alpha = a\omega/U$. More details about equations (3–6) are given by Badr (1994b). The present study focuses only on the two symmetric flow cases: $\lambda = 0$ and $\lambda = 90^\circ$. In the case without inclination ($\lambda = 0$) the flow is symmetric about the major axis, whereas in the second ($\lambda = 90^\circ$) the flow is symmetric about the minor axis. In the present analysis the calculations are carried out on the basis of the method of solution adopted by Badr (1994b) in which the functions ψ and ζ were expressed in the form of Fourier series

$$\psi = \sum_{n=1}^{N} [f_n(\xi, t) \sin n\eta + F_n(\xi, t) \cos n\eta], \quad \zeta = \sum_{n=1}^{N} [g_n(\xi, t) \sin n\eta + G_n(\xi, t) \cos n\eta] \tag{7a, b}$$

In the case of symmetrical flow about the major axis, the functions $F_n(\xi, t)$ and $G_n(\xi, t)$ are identically zero in (7); whereas in the case of symmetrical flow about the minor axis, the functions $f_{2p-1}(\xi, t)$, $F_{2p}(\xi, t)$, $g_{2p-1}(\xi, t)$ and $G_{2p}(\xi, t)$ for all integers $p \geq 1$, are identically zero in (7). This is due to the fact that in the first case the flow is symmetric about $\eta = 0$, whereas in the second the flow is symmetric about $\eta = 90^\circ$. The equations governing the functions in (7a, b) can be obtained by substitution in (3) and (4). They have been given by Badr (1994b) and their solution is required in the present case subject to the conditions

$$f_n = \frac{\partial f_n}{\partial \xi} = F_n = \frac{\partial F_n}{\partial \xi} = 0 \quad \text{when} \quad \xi = \xi_0 \tag{8a}$$

$$g_n, G_n \to 0 \quad \text{as} \quad \xi \to \infty \tag{8b}$$

$$f_n \to \frac{c}{2} \delta_{n1} e^{\xi} \cos \lambda \cos \alpha t, \quad \frac{\partial f_n}{\partial \xi} \to \frac{c}{2} \delta_{n1} e^{\xi} \cos \lambda \cos \alpha t \quad \text{as} \quad \xi \to \infty \tag{8c}$$

$$F_n \to -\frac{c}{2} \delta_{n1} e^{\xi} \sin \lambda \cos \alpha t, \quad \frac{\partial F_n}{\partial \xi} \to -\frac{c}{2} \delta_{n1} e^{\xi} \sin \lambda \cos \alpha t \quad \text{as} \quad \xi \to \infty \tag{8d}$$

Here δ_{n1} is the Kronecker delta symbol defined by $\delta_{n1} = 1$ if $n = 1$, and $\delta_{n1} = 0$ if $n \neq 1$.

It may be shown that conditions (8) can be combined to give a further set of conditions of global type, namely

$$\int_{\xi_0}^{\infty} \left[\left(\frac{c}{2} \cosh 2\xi \right) g_n - \frac{c}{4} (\operatorname{sgn}(n-2) g_{|n-2|} + g_{n+2}) \right] e^{-n\xi} d\xi = \delta_{n1} \cos \lambda \cos \alpha t \tag{9a}$$

$$\int_{\xi_0}^{\infty} \left[\left(\frac{c}{2} \cosh 2\xi \right) G_n - \frac{c}{4} G_{|n-2|} + G_{n+2}) \right] e^{-n\xi} d\xi = -\delta_{n1} \sin \lambda \cos \alpha t \tag{9b}$$

In the initial stages of the motion, the boundary-layer coordinate x can be introduced by the transformation,

$$\xi = \xi_0 + kx, \quad k = 2(2\tau/\mathrm{Re})^{1/2}, \quad \tau = t \tag{10}$$

This is employed to transform all the appropriate equations with the scaling of the variables,

$$F_n = kF_n^*, \quad G_n = \frac{G_n^*}{k}, \qquad f_n = kf_n^*, \quad g_n = \frac{g_n^*}{k} \tag{11}$$

Here k denotes the growth of the boundary-layer structure of the initial flow (small time). This change of variables stretches the thin boundary-layer and scales the stream function and vorticity so that they are of order unity. This transformation has been used by several authors, some of whom include Collins & Dennis (1973), Badr & Dennis (1985), Badr (1994b), Badr *et al.* (1995a, b), Nguyen & Kocabiyik (1996). It is noted that the physical coordinate $\xi = \xi_0 + kx$ is a moving coordinate, and hence the outer boundary $\xi_{\max} = \xi_0 + kx_{\max}$ is constantly being pushed further away from the cylinder surface at a rate which reflects the growth of the boundary-layer. For this reason we are justified in saying that the vorticity, by the mechanism of convection, does not reach the outer boundary $\xi_{\max}$. Here, $\xi_{\max}$ refers to the outer boundary approximating infinity.

3. NUMERICAL INTEGRATION PROCEDURE

The numerical method implemented to calculate the flow for any Reynolds number and large enough time is similar to that outlined in Badr (1994b) and will briefly be described. In this method, the velocity of the free stream starts *suddenly* from rest at time $t = 0$. Immediately following the start of fluid motion, a very thin boundary layer develops over the cylinder surface and grows with time. Accordingly, the solution time is divided into two distinct zones. The first zone begins following the start to fluid motion and continues until the boundary layer becomes thick enough to use the elliptic coordinates (ξ, η). In this zone the boundary-layer coordinates are used, which are appropriate to the flow-field structure, in order to obtain a highly accurate numerical solution. The second zone starts following the first one and continues until the termination of calculations.

The governing equations and the boundary and integral conditions (8) and (9) are first transformed to the coordinate system (10). To initiate the integration procedure, the initial solution obtained by Staniforth (1972) at $t = 0$ is used, after some modification to suit the dimensionless variables used in this work. This initial solution is given by

$$\psi^* = e^{\xi_0} \sin(\eta - \lambda)\left[x \operatorname{erf}(H_0^{1/2}x) + \frac{1}{\pi^{1/2}H_0^{1/2}} (\mathrm{e}^{-H_0x^2} - 1) \right] \tag{12a}$$

$$\zeta^* = \frac{2\mathrm{e}^{\xi_0}}{\pi^{1/2}H_0^{1/2}} \sin(\eta - \lambda)\mathrm{e}^{-H_0x^2} \tag{12b}$$

where $H_0 = \frac{1}{2}(\cosh 2\xi_0 - \cos 2\eta)$. The use of the initial solution (12) is essential for obtaining accurate results at small times. An implicit method of the Crank-Nicolson type is used to integrate the governing equations in time, following the work by Badr (1994b). The solution procedure requires knowledge of the surface vorticity distribution. The integral conditions (9) are used to calculate the values of the functions g_n and G_n on the cylinder surface $(\xi = \xi_0)$ from which the required surface vorticity distribution can be obtained at

every time step. Following the start of fluid motion, very small time steps ($\Delta\tau = 10^{-4}$) are taken, since the time variation of the vorticity field is quite fast. However, as time increases, the time step was gradually increased until it reached $\Delta\tau = 0{\cdot}05$. The number of points in the ξ direction is taken as 101 with a space step of $\Delta\xi = 0{\cdot}1$. This makes $\xi_{\max} = \xi_0 + 10$, which sets the outer boundary at a physical distance of more than 10^4 times the focal distance. Such a far-away boundary ensures that the application of boundary conditions (8a)–(8d) does not affect the solution in the viscous region near the cylinder surface. The number of terms in the series (7a) and (7b) starts with 15 at $t = 0$ and more terms are added as time increases. One more term is added at a time when the last term in the series reaches a maximum value of 10^{-4}. For the range of Reynolds number considered in this paper, a maximum of 30 terms is found adequate over the large time range of calculations.

4. RESULTS AND DISCUSSION

The variation of drag coefficients with time is calculated both from the viscous flow and inviscid flow solutions. It may be noted that the present analysis uses the analytical expressions for the surface pressure and drag coefficient obtained by Badr (1994a) in the case of oscillating inviscid flow. A dimensionless drag coefficient C_D is defined by

$$C_D = \frac{D}{\frac{1}{2}\rho U_0^2 (2a)}$$

where D is the total drag on the cylinder. The above expression can be split into two parts, one due to frictional forces and the other due to pressure forces. The resulting coefficients can be expressed in terms of the Fourier functions as

$$C_{DF} = \frac{2\pi}{\mathrm{Re}} [(\cos\lambda) g_1 - \tanh\xi_0 (\sin\lambda) G_1]_{\xi_0} \tag{13a}$$

$$C_{DP} = \frac{2\pi}{\mathrm{Re}} \left[(\sin\lambda) \frac{\partial G_1}{\partial \xi} - \tanh\xi_0 (\cos\lambda) \frac{\partial g_1}{\partial \xi} \right]_{\xi_0} \tag{13b}$$

where C_{DF} and C_{DP} are the frictional and pressure components of the drag coefficient respectively. The inviscid flow properties can be obtained by solving the unsteady Euler equation for the special case under consideration in which the free-stream velocity changes according to $U \cos \omega t^*$. The inviscid force coefficient given by Badr (1994a) is in the form

$$C_D(\xi_0, \lambda, \alpha, t) = -\frac{\pi\alpha e^{\xi_0} \sin\alpha t}{\cosh\xi_0} [\tanh\xi_0 \cos^2\lambda + \sin^2\lambda] \tag{14}$$

The calculated values of C_{DF} and C_D based on expressions (13) and (14) are plotted in Figures 1–3 for comparison with inviscid flow when the flow is symmetric about either the major axis ($\lambda = 0$) or the minor axis ($\lambda = 90^\circ$). The variation of C_D with time for the cases of $\mathrm{Re} = 500$, $b/a = 0{\cdot}8$, $\alpha = \pi/4, \pi/2$ and $\mathrm{Re} = 10^3$, $b/a = 0{\cdot}8$, $\alpha = \pi/4, \pi/2$ are shown in Figures 1 and 2.

These figures show that the contribution of frictional forces to the total drag coefficient C_D is relatively small. They also show that the phase difference between the viscous and inviscid flow solutions is small at the start of the motion and increases with the increase of time. The reason for this is that the flow field away from the cylinder is vortex-free at small times. As time increases, vortices are shed away from the cylinder, causing changes in the

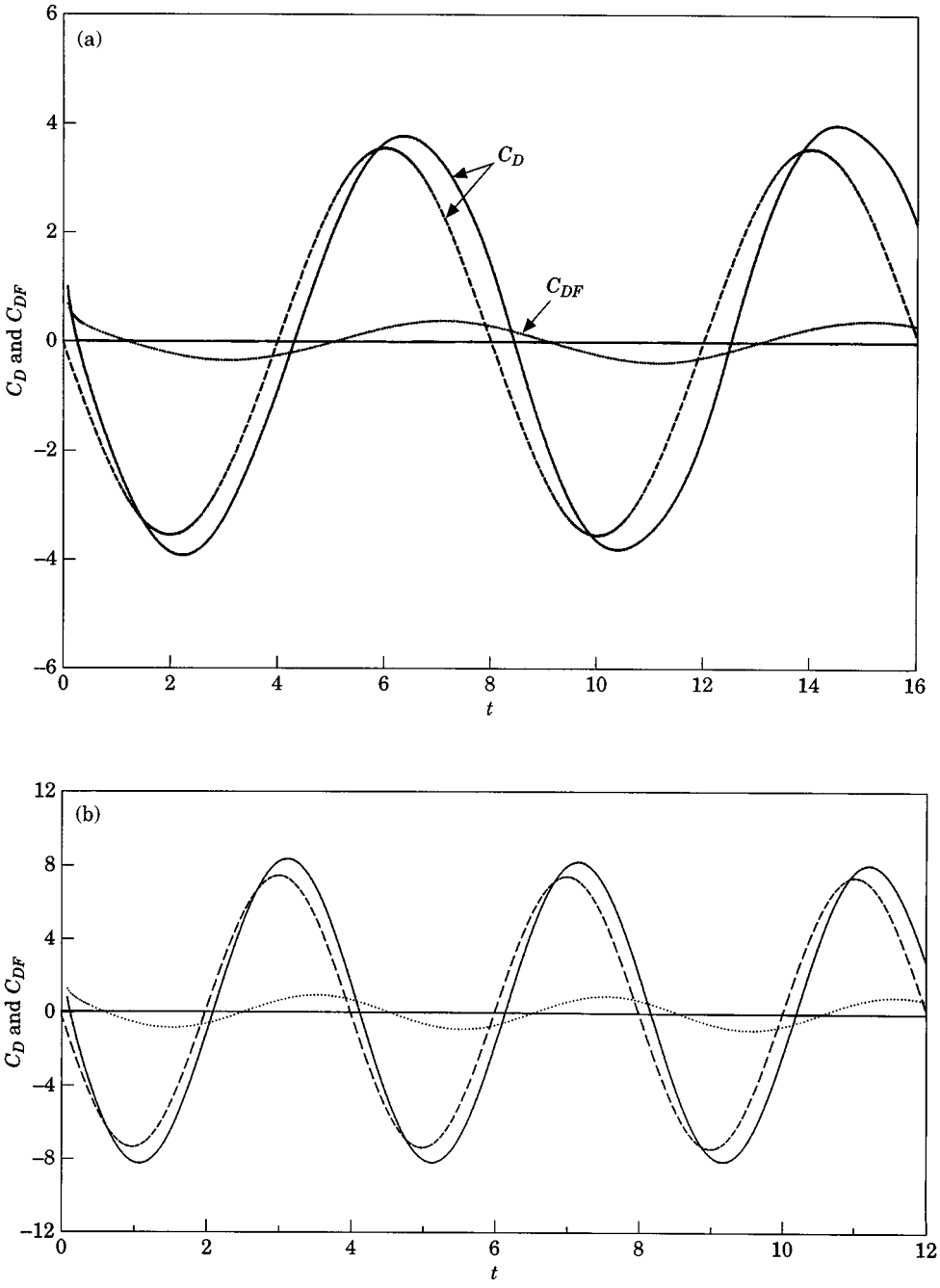

Figure 1. The time variation of C_{DF} and C_D following the start of oscillating flow; case of Re = 500, $b/a = 0{\cdot}8$, $\lambda = 0^\circ$ when (a) $\alpha = \pi/4$ and (b) $\alpha = \pi/2$: ——, C_D present study; … , C_{DF} [equation (13a)]; – – – , C_D for potential flow [equation (14)].

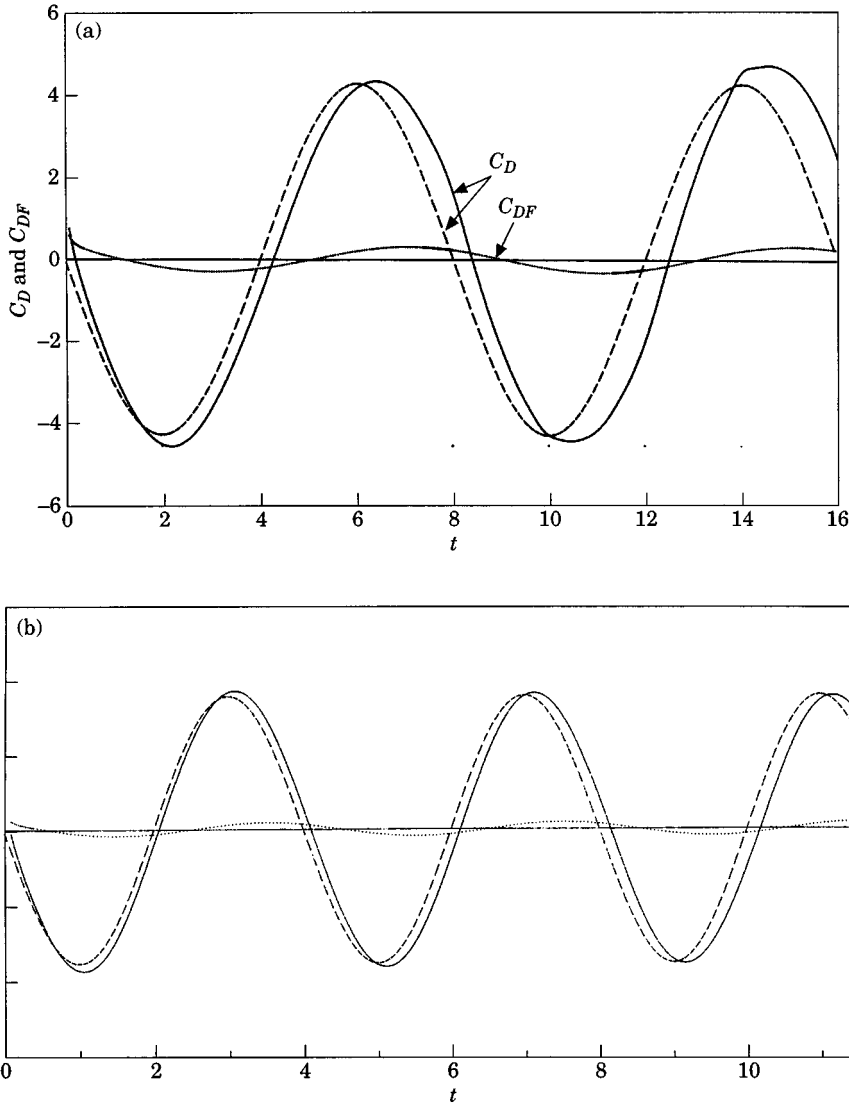

Figure 2. The time variation of C_{DF} and C_D following the start of oscillating flow; case of Re $= 10^3$, $b/a = 0{\cdot}8$, $\lambda = 0°$ when (a) $\alpha = \pi/4$ and (b) $\alpha = \pi/2$: ——, C_D present study; … , C_{DF} [equation (13a)]; – – – , C_D for potential flow [equation (14)].

flow-field structure. Such changes will cause the flow away from the cylinder to deviate from the potential flow. Accordingly, one can assume that there are two dominating flow fields affecting the boundary-layer region. The first is the potential flow field, while the second (superimposed on the first) is that resulting from vertical motion. In the present problem the second field has negligible effect at the start of fluid motion but with increasing influence as time increases. Such a field continues to evolve with time until asymptotically approaching a periodic behaviour at large time. The time variation of C_D for the case of Re $= 500$, $b/a = 0{\cdot}8$ and $\alpha = \pi/4$ is shown in Figure 3(a) when the free stream is parallel to the minor

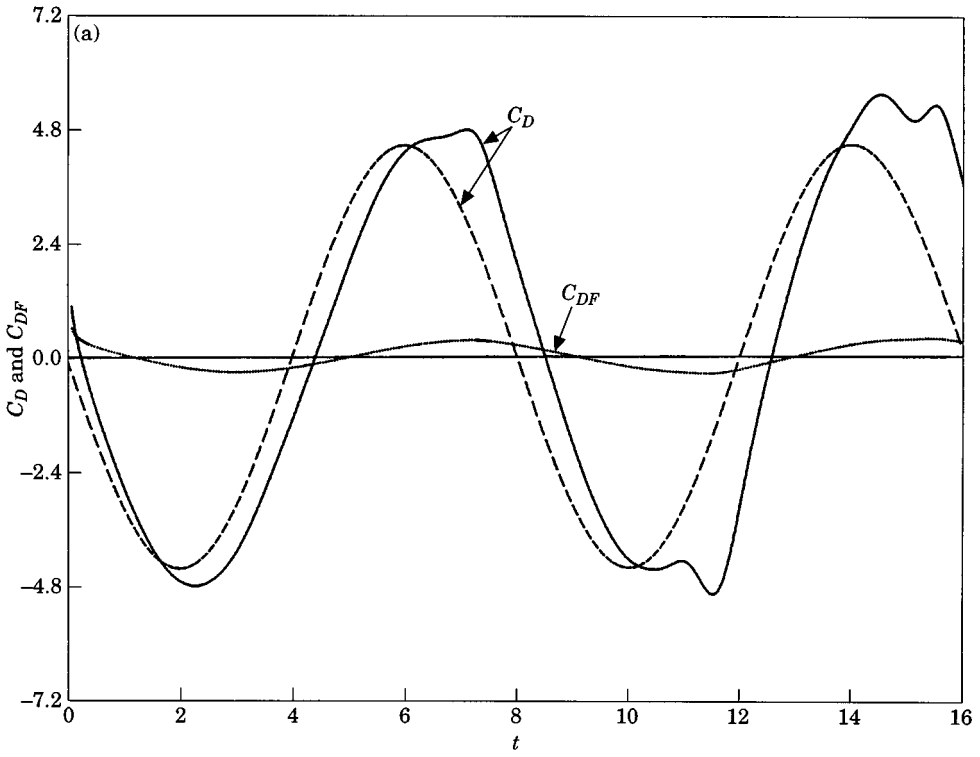

Figure 3(a). The time variation of C_{DF} and C_D during two complete cycles following the start of oscillating flow for the case of Re = 500, $b/a = 0{\cdot}8$, $\lambda = 90^\circ$ and $\alpha = \pi/4$; ——, C_D present study; … , C_{DF} [equation (13a)]; – – – , C_D for potential flow [equation (14)].

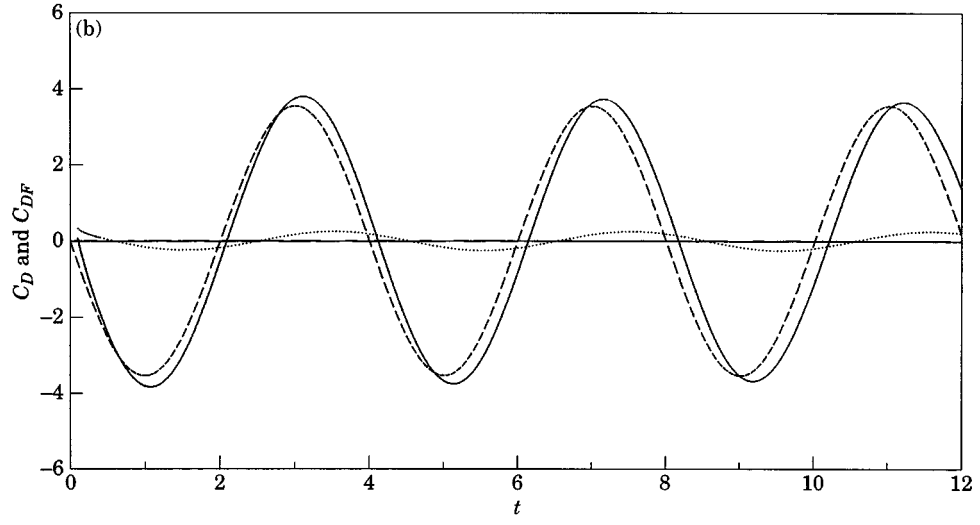

Figure 3(b). The time variation of C_{DF} and C_D following the start of oscillating flow for the case of Re = 500, $b/a = 0{\cdot}5$, $\lambda = 0^\circ$ and $\alpha = \pi/2$; ——, C_D present study; … , C_{DF} [equation (13a)]; – – – , C_D for potential flow [equation (14)].

axis ($\lambda = 90°$). Potential flow solutions for the same coefficient are shown in the figure. Figures 1(b), 2(b) and 3(b) show a small difference between the values of C_D obtained from viscous and inviscid flow solutions. This is expected since the flow oscillations in this case exhibit high frequency and a relatively low amplitude. The effect of both factors is simply an increase of the inertia effect and a decrease in the size of the separated flow region. Both effects will create a pressure field closer to that of potential flow.

In order to plot the surface pressure distribution, we introduce the dimensionless pressure coefficient p^*, defined as

$$p^*(\eta, \tau) = \frac{p_\eta - p_\pi}{\frac{1}{2}\rho U_0^2}$$

It can be shown that the surface pressure for the viscous flow is given by

$$p^*(\eta, \tau) = -\frac{4}{\mathrm{Re}} \left\{ \sum_{n=1}^{N} \frac{1}{n} \left[\frac{\partial G_n}{\partial \xi} \sin n\eta - \frac{\partial g_n}{\partial \xi} (\cos n\eta - \cos n\pi \right] \right\} \tag{15}$$

following Badr (1994b). For inviscid flow, the surface pressure coefficient is deduced from the analysis of Badr (1994a).

$$p^*(\eta, \tau) = 2\alpha c e^{\xi_0} \sin \alpha t [\cos(\eta - \lambda) + \cos \lambda] + e^{2\xi_0} (\cos^2 \alpha\tau) F(\eta)$$

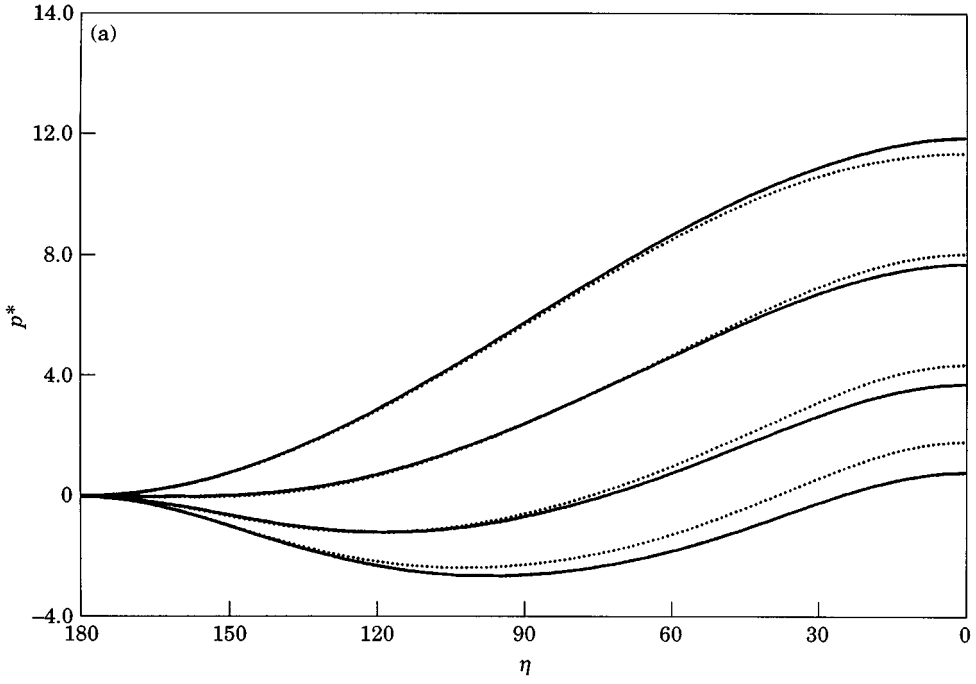

Figure 4(a). The surface pressure distribution at time $t = 0{\cdot}1, 0{\cdot}25, 0{\cdot}5, 1{\cdot}0$ following the start of the oscillating flow for the case of re $= 500$, $b/a = 0{\cdot}8$, $\lambda = 0°$ and $\alpha = \pi/2$ and comparison with the potential flow solution: ——, present study; … , potential flow (Badr 1994a).

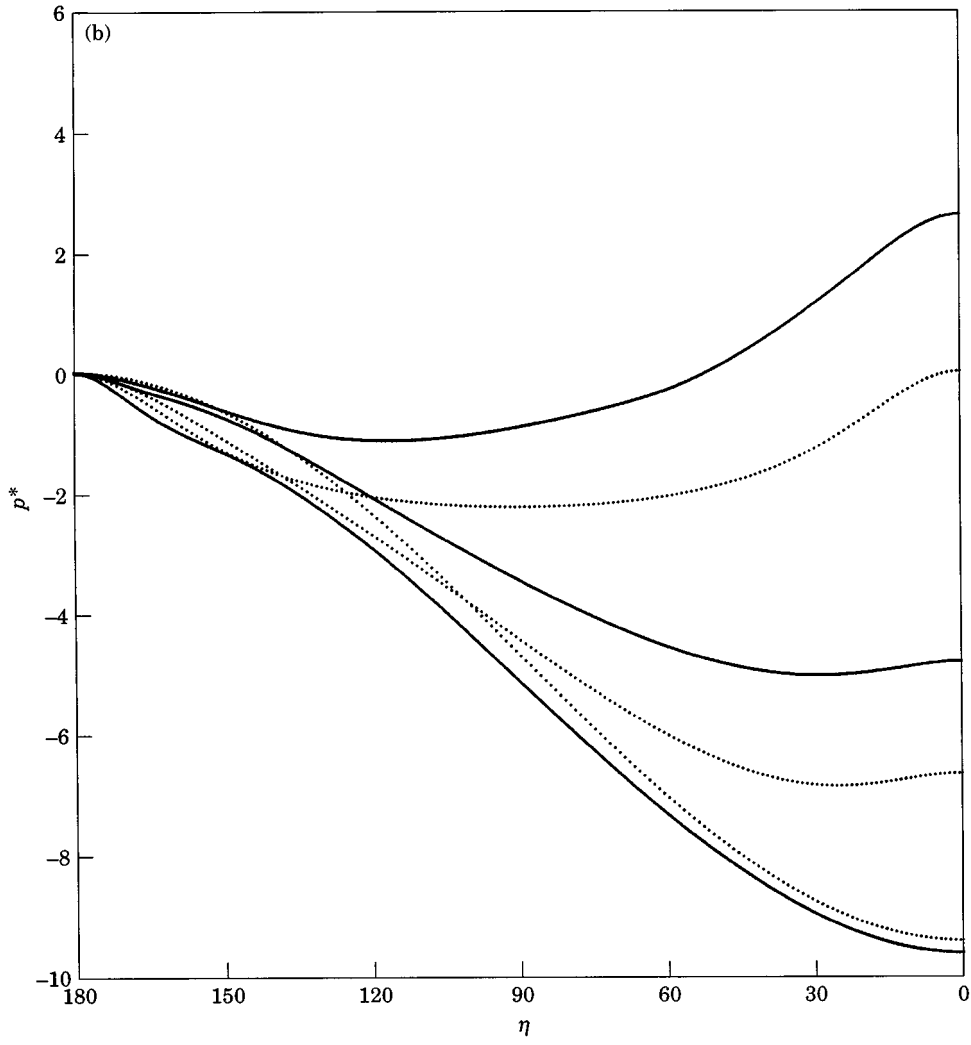

Figure 4(b). The surface pressure distribution during one quarter of a complete oscillation at times $t = 10, 10{\cdot}5,$ and 11 for the case of Re = 500, $b/a = 0{\cdot}5$, $\lambda = 0^\circ$ and $\alpha = \pi/2$: ——, present study; … , potential flow (Badr 1994a).

where $F(\eta)$ is given by

$$F(\eta) = \int_0^\eta \left(\frac{\sin^2(\eta - \lambda) \sin 2\eta}{(\cosh^2 \xi_0 - \cos^2 \eta)^2} - \frac{\sin 2(\eta - \lambda)}{\cosh^2 \xi_0 - \cos^2 \eta} \right) \mathrm{d}\eta$$

The value of the function $F(\eta)$ is to be calculated for any given angle η using numerical integration. Figures 4(a) and 4(b) show the time variation of the pressure distribution for the case of Re = 500, $\alpha = \pi/2$, and $b/a = 0{\cdot}8$ and $0{\cdot}5$, respectively, when the flow is symmetric about the major axis ($\lambda = 0$). On the same figures the corresponding inviscid flow solution for the surface pressure distributions are also plotted. The comparison given in Figure 4(a) shows a good agreement at early stages of the flow. Figure 4(b) shows the time variation of the surface pressure distribution during one-quarter of a complete oscillation. It is

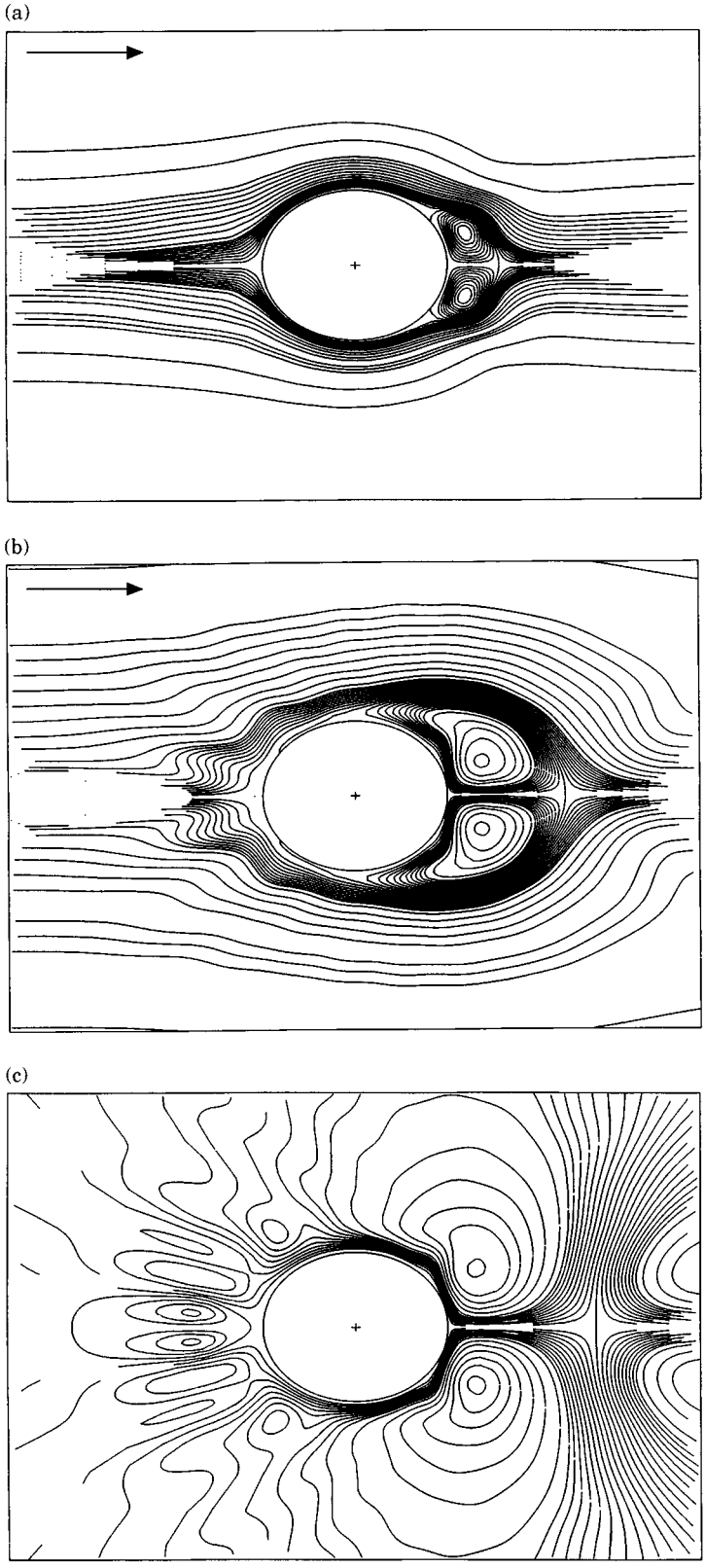

Figure 5. The streamline pattern during one complete oscillation for the case of $\mathrm{Re} = 10^3$, $b/a = 0{\cdot}8$, $\lambda = 0^\circ$ and $\alpha = \pi/4$ at times (a) $t = 8{\cdot}0$, (b) $t = 9{\cdot}5$, (c) $t = 10{\cdot}0$, (d) $t = 12{\cdot}0$, (e) $t = 13{\cdot}0$, (f) $t = 13{\cdot}8$, (g) $t = 14{\cdot}0$, (h) $t = 16{\cdot}0$.

(d)

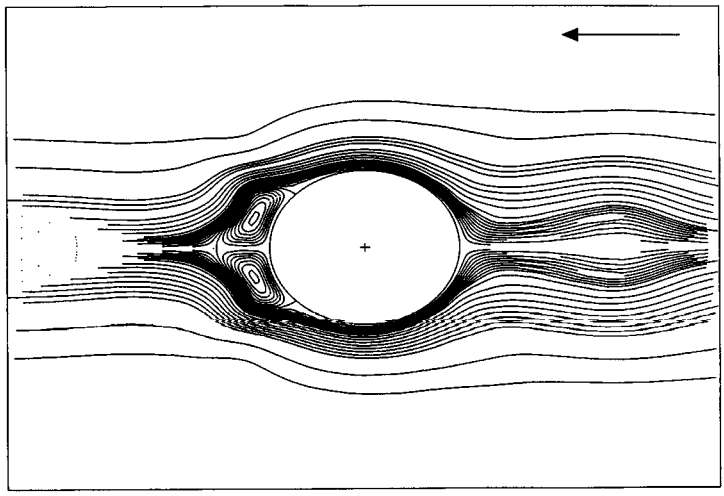

(e)

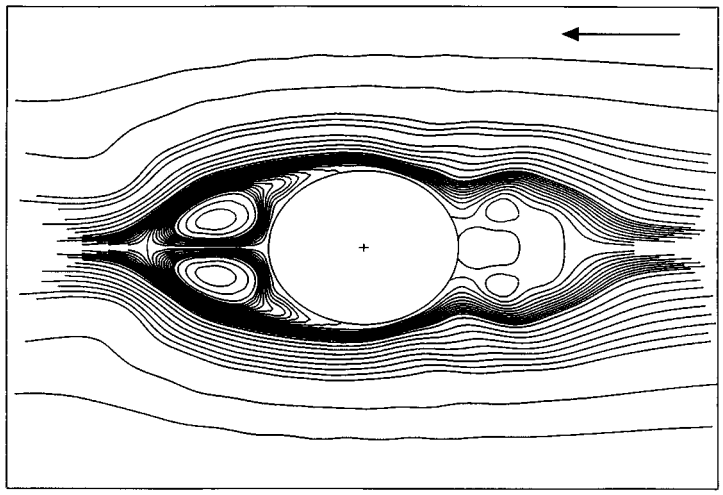

(f)

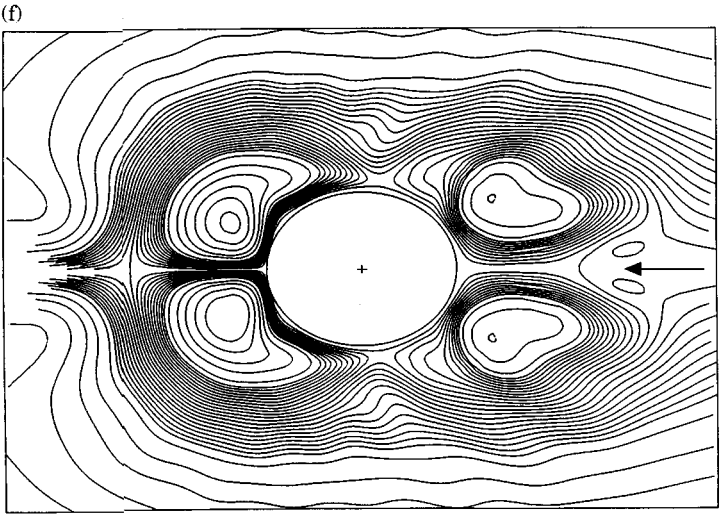

Figure 5. (*Continued*).

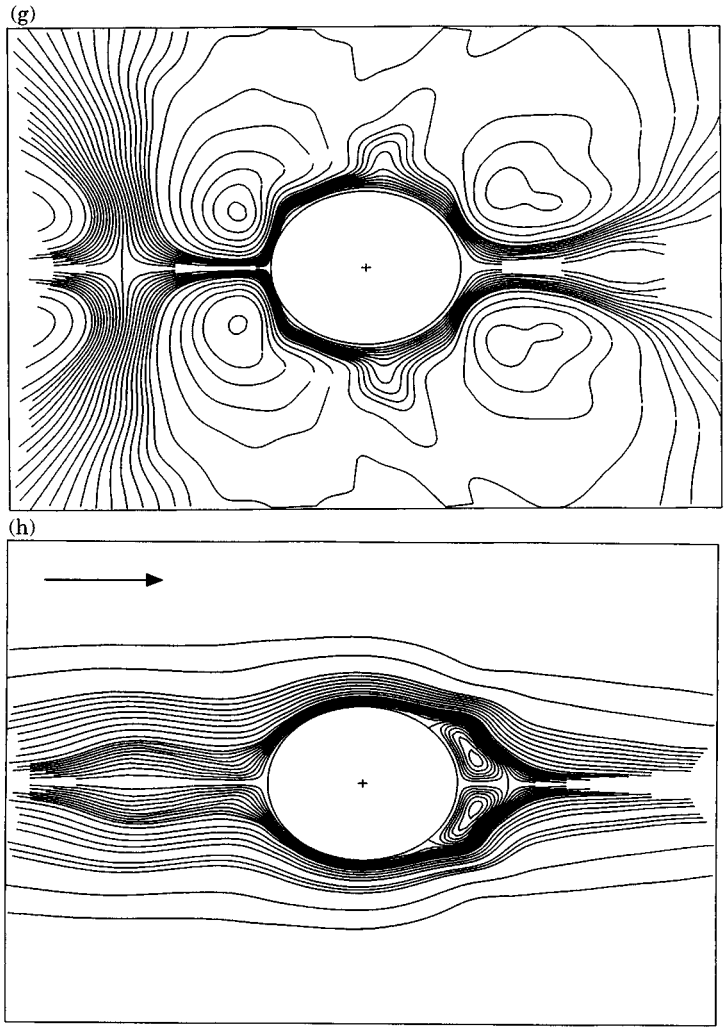

Figure 5. (*Continued*).

important to mention that the curve for $t = 10$ corresponds to $U = U_{max}$ at which the inertia effect is zero, and that for $t = 11$ corresponds to $U = 0$ at which the inertia effect is maximum. As can be seen in Figure 4(b), the viscous and inviscid flow pressure distributions are in good agreement over most of the cylinder surface at $t = 11$ (corresponding to zero free-stream velocity and maximum inertia effect).

The instantaneous streamline patterns are plotted for the two cases of $\mathrm{Re} = 10^3$, $b/a = 0{\cdot}8$, $\alpha = \pi/4$ and $\pi/2$ when the flow is symmetric about the major axis ($\lambda = 0$). Figure 5 shows the time variation of the streamline pattern for the first case when t varies from 8·0 to 16·0. This gives the details of the flow field structure during the second oscillation after the start of fluid motion. Figure 5(a) shows the streamlines when the free stream is moving to the right at maximum velocity. The figure shows a pair of vortices growing in the cylinder wake. One can see the growth of this vortex pair in the cylinder

wake in Figure 5(b). Figure 5(c) shows the streamlines when the free-stream velocity is zero. The large distances between streamlines far away from the cylinder reflect the very small velocity there, while the fluid motion near the cylinder is dominated by vortical motion. Figure 5(d) shows the situation when the free stream is moving to the left at maximum velocity. The figure is very much the same as Figure 5(a), only turned through an angle of 180° since the free stream has completed one half-cycle of oscillation. Figures 5(e)–5(f) give additional details of the flow structure as the free stream decelerates before reversing direction at $t = 14{\cdot}0$. Figure 5(g), which shows the streamline pattern when the free-stream velocity is zero, is very much the same as Figure 5(c) when turned through an angle of 180°. Finally, Figure 5(h), which shows the flow field at the end of the second complete oscillation ($t = 16{\cdot}0$), is similar to the situation at the beginning of that oscillation ($t = 8{\cdot}0$) shown in Figure 5(a). The minor differences between Figures 5(a) and 5(h) reflect the continuous development of the flow field away from the cylinder because of the vortex shedding and interaction with the free stream. This flow field has not yet become periodic and requires a large number of oscillations before reaching the quasi-steady state.

The time variation of the streamline pattern for the case of $\mathrm{Re} = 10^3$, $b/a = 0{\cdot}8$, $\alpha = \pi/2$ when the flow is symmetric about the major axis ($\lambda = 0$) is shown in Figures 6(a)–(h) for selected values of t between $t = 8{\cdot}0$ and $t = 12{\cdot}0$. The chosen interval represents the third complete oscillation following the start of fluid motion. Figures 6(a), 6(c) and 6(h) represent the situation at the beginning, middle and end of the oscillation, respectively. The velocity of the free stream is maximum in each of these figures. On the other hand, Figures 6(b) and 6(f) represent the times at which the free-stream velocity is zero. Streamline patterns in Figure 6 show that vortices are formed in relatively small areas, leaving the rest of the flow vortex-free. The repetitive nature of the flow field can be observed from the mirror image resemblances between the diagrams for $t = 8{\cdot}0$ and $t = 10{\cdot}0$; $t = 9{\cdot}0$ and $t = 11{\cdot}0$. These are given in Figures 6(a) and 6(c); 6(b) and 6(f). Since vortex shedding is restricted to a very small region, the pressure distribution becomes very close to that of potential flow, which explains the behaviour of C_D presented in Figure 2(b). Figures 6(a) and 6(h) are almost the same, showing the periodic variation of the flow field at $t = 8{\cdot}0$ and $t = 12{\cdot}0$, respectively.

The instantaneous streamline patterns are plotted for the same of $\mathrm{Re} = 500$, $b/a = 0{\cdot}8$, $S = \pi/4$ when the flow is symmetric about the minor axis ($\lambda = 90°$) in Figures 7(a)–(h) for only selected values of t between $t = 8{\cdot}0$ and $t = 16{\cdot}0$. This gives the details of the flow-field structure during the second oscillation after the start of the motion. During the first quarter of this cycle the free stream is moving to the right (see Figures 7(a, b)). In Figure 7(a) the velocity of the free stream in maximum, whereas in Figure 7(c) free-stream velocity is zero. Figure 7(d), at $t = 12{\cdot}0$, shows the situation at the middle of the oscillation and the free stream is moving to the right at maximum velocity. Figures 7(e) and 7(f) give additional details of the flow structure as the free stream decelerates before reversing the direction at $t = 14{\cdot}0$. Figure 7(f), at $t = 13{\cdot}8$, shows the streamline pattern before the free stream comes to complete rest. Figure 7(g), at $t = 14{\cdot}0$, represents the time at which the free-stream velocity is zero. Finally, Figure 7(h) shows the flow field at the end of the second complete oscillation ($t = 16{\cdot}0$). The repetitive nature of the flow field can be observed from the mirror image resemblances between the diagrams for $t = 8{\cdot}0$ and $t = 12{\cdot}0$; $t = 10{\cdot}0$ and $t = 14{\cdot}0$; $t = 12{\cdot}0$ and $t = 16{\cdot}0$. These are given in Figures 7(a) and 7(d); 7(c) and 7(g); 7(d) and 7(h). Figure 7(a) and 7(h) are almost the same, showing the periodic variation of the flow field at $t = 8{\cdot}0$ and $t = 16{\cdot}0$, respectively; small deviations between the streamline patterns are due to the fact that the numerical solution was not advanced far enough in time to achieve a periodic flow field.

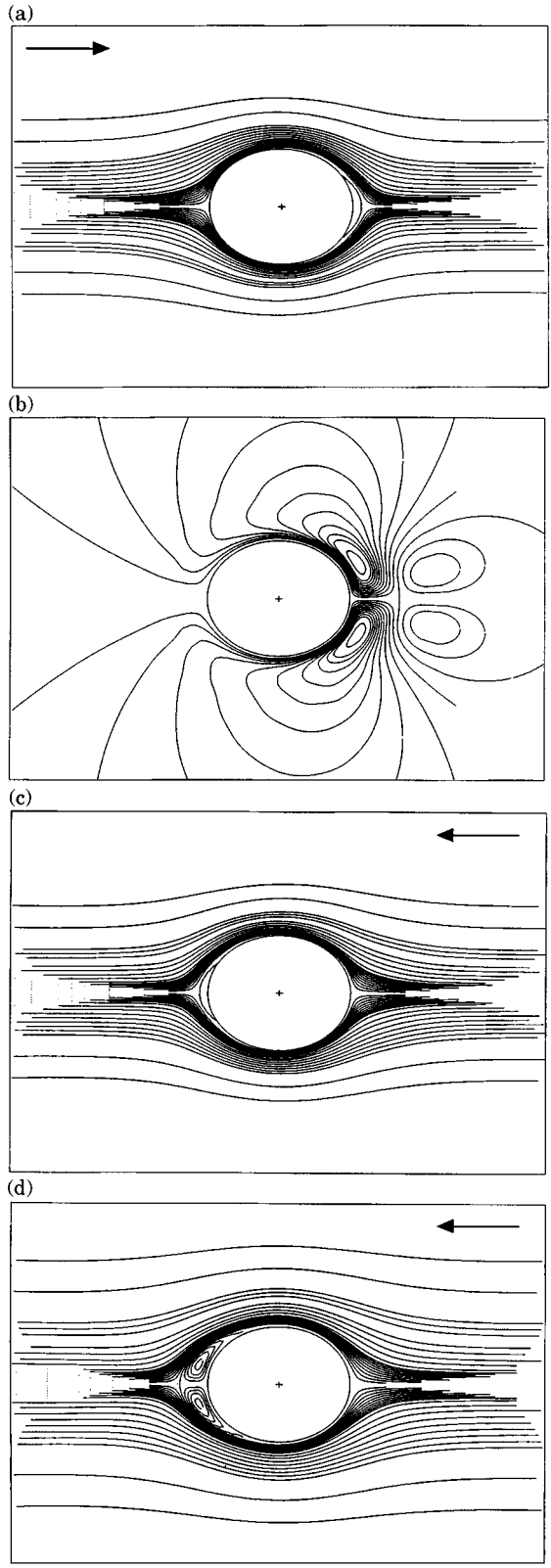

Figure 6. The streamline pattern during one complete oscillation for the case of $\mathrm{Re} = 10^3$, $b/a = 0{\cdot}8$, $\lambda = 0^\circ$ and $\alpha = \pi/2$ at times (a) $t = 8{\cdot}0$, (b) $t = 9{\cdot}0$, (c) $t = 10{\cdot}0$, (d) $t = 10{\cdot}5$, (e) $t = 10{\cdot}9$, (f) $t = 11{\cdot}0$, (g) $t = 11{\cdot}5$, (h) $t = 12{\cdot}0$.

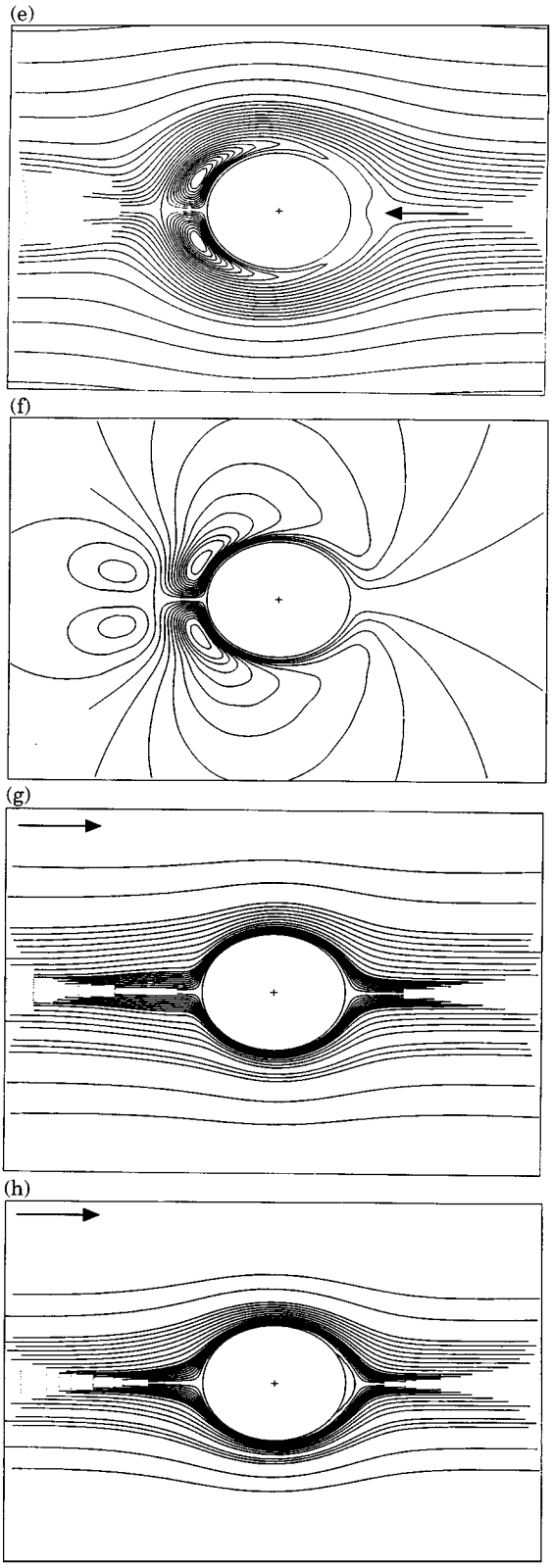

Figure 6. (*Continued*).

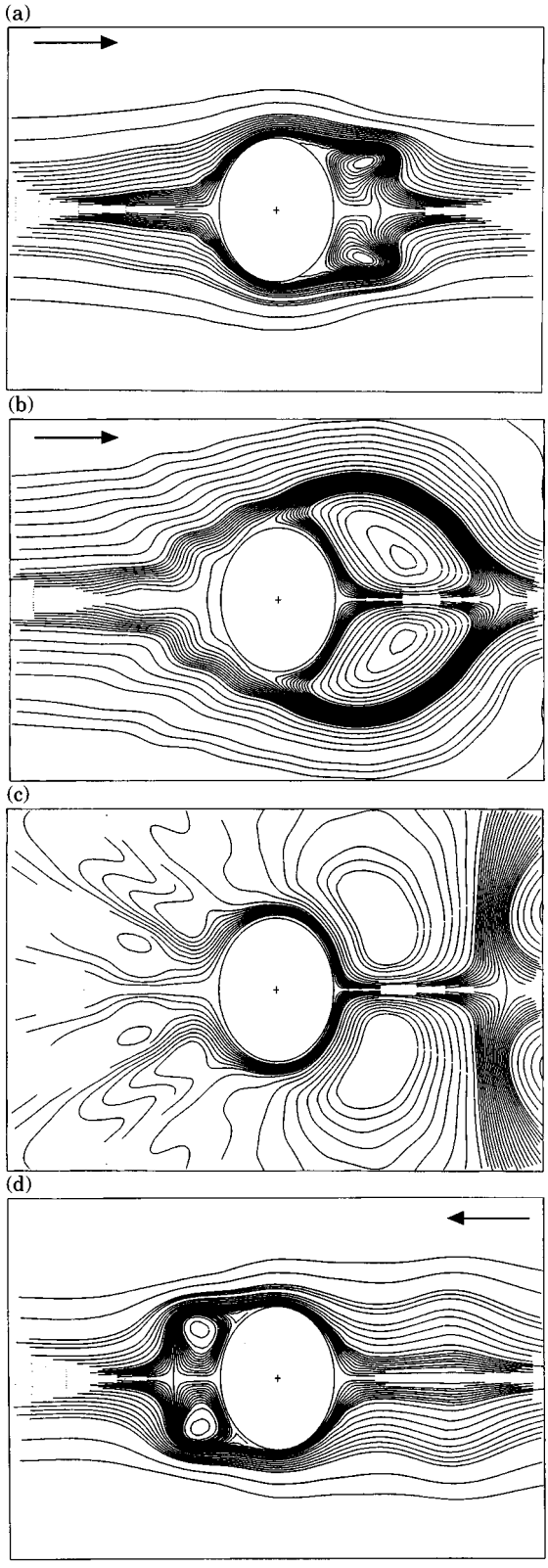

Figure 7. The streamline pattern during one complete oscillation for the case of Re = 500, $b/a = 0{\cdot}8$, $\lambda = 90^\circ$ and $\alpha = \pi/4$ at times (a) $t = 8{\cdot}0$, (b) $t = 9{\cdot}5$, (c) $t = 10{\cdot}0$, (d) $t = 12{\cdot}0$, (e) $t = 13{\cdot}0$, (f) $t = 13{\cdot}8$, (g) $t = 14{\cdot}0$, (h) $t = 16{\cdot}0$.

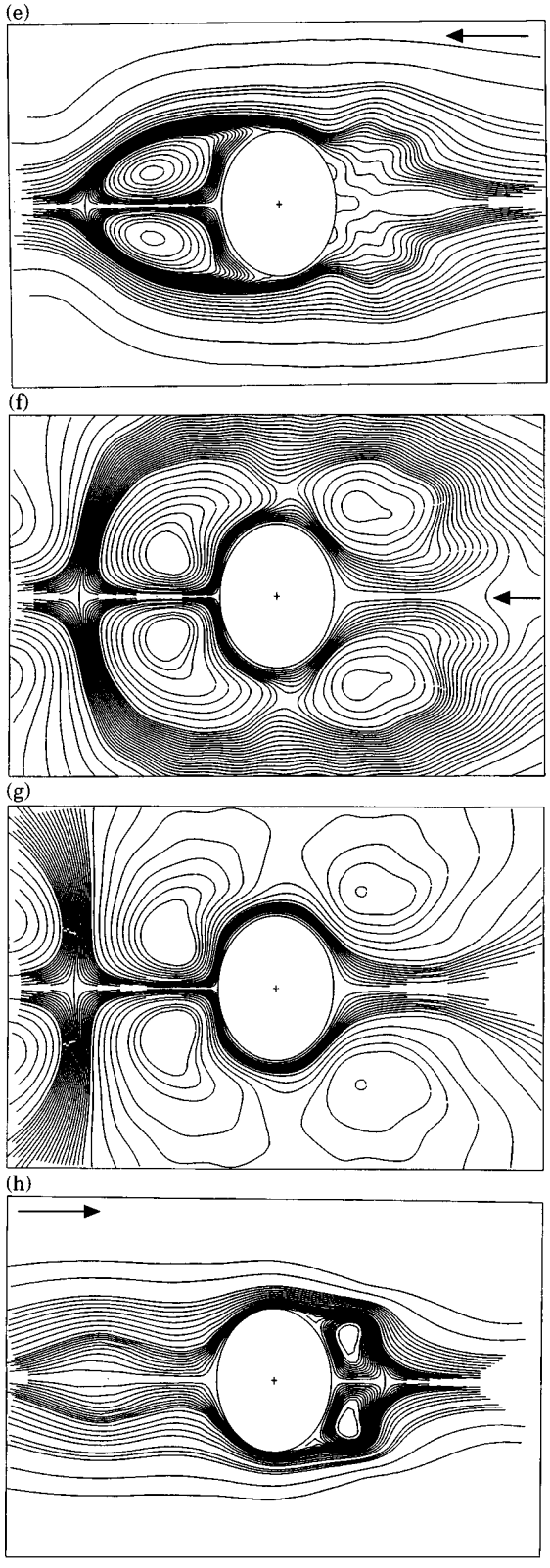

Figure 7. (*Continued*).

The accuracy of the method of solution and the numerical scheme used in this work is checked by applying it to the problem of an elliptic cylinder starting its translational constant velocity motion impulsively from rest in a fluid of infinite extent (this case corresponds to $\alpha = 0$ in the present study). Patel (1981) made a numerical study on the flow development near an elliptic cylinder starting its motion impulsively, in the Reynolds number range from 60 to 200. Honji (1972) carried out experiments on both asymmetric and symmetric flow problems for the case of the impulsively started translating elliptic cylinder. Figure 8 shows a comparison between the time variation of the dimensionless wake length, L/c, obtained by using the present scheme and numerical results of Patel (1981) and also by using flow visualization results of Honji (1972) in the case of symmetric flow about the major axis ($\lambda = 0$) when Re $= 200$, $b/a = 0{\cdot}588$. The figure shows a good agreement between the three sets of results.

Figure 9 shows a comparison between the time variation of C_D obtained using the present scheme and that obtained numerically by Patel (1981) in the case of symmetric flow about the major axis ($\lambda = 0$) when Re $= 200$, $b/a = 0{\cdot}588$. It is important to note that the discrepancy between the results of C_D at small times is due to the fact that Patel used a potential flow solution as an initial condition, whereas the present study uses the exact solution (12) as an initial condition. As mentioned earlier, the use of initial solution (12) is essential for obtaining accurate results at small times. It is also noted that in Patel's work no measures were taken to ensure the periodicity of pressure.

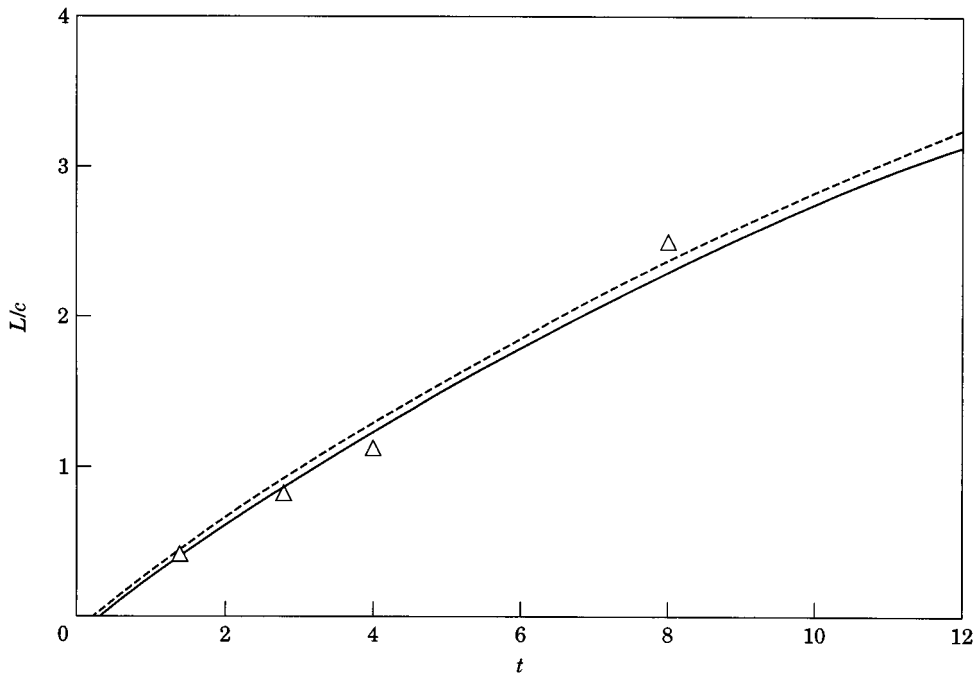

Figure 8. The time development of the dimensionless wake length (L/c) for the case of Re $= 200$, $\lambda = 0°$ and $b/a = 0{\cdot}588$; ——, present study; – – –, Patel (1981); Δ, Honji (1972).

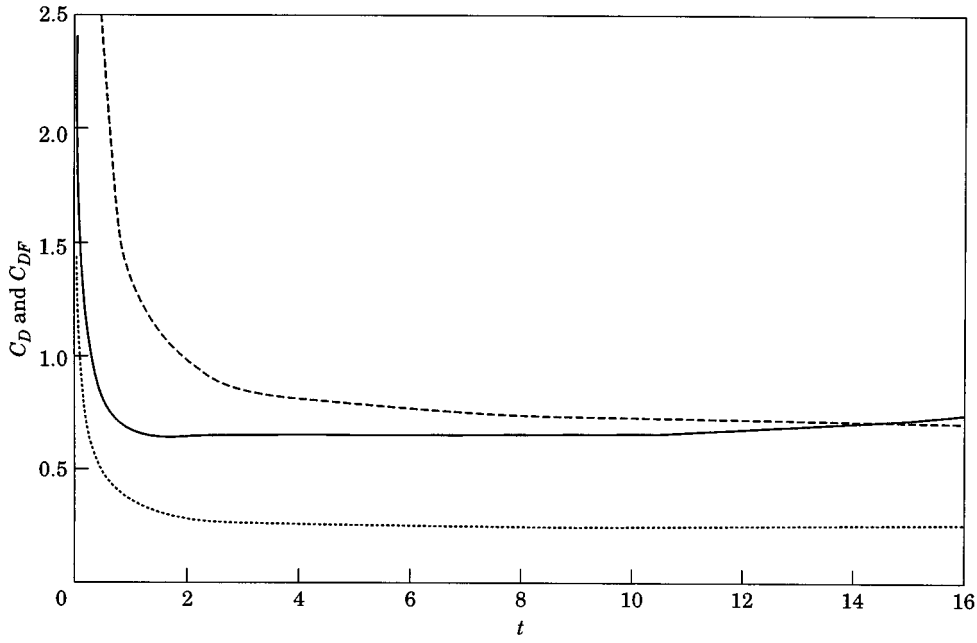

Figure 9. The time development of C_{DF} and C_D following impulsive start of motion and comparison with Patel (1981) for the case of Re (based on 2c) = 200: ——, C_D; ... , C_{DF} [equation (13a)]; – – – , C_D (Patel 1981).

5. CONCLUSIONS

Considered in this paper is the problem of oscillating viscous flow over a stationary elliptic cylinder for Reynolds numbers of 200, 500 and 1000. Attention is focused upon only two symmetric flow cases. In the first, flow is symmetric about the major axis whereas in the second, flow is symmetric about the minor axis. The solution is based on a numerical integration of the vorticity transport equation together with the stream function equation. A boundary-layer coordinate system is used following the start of fluid motion to ensure high accuracy at small times. Integral conditions were deduced and used in the numerical scheme for accurate prediction of vorticity components at the solid boundary. The methods of solution and numerical scheme are verified by applying them to the special case of an elliptic cylinder starting its constant velocity motion impulsively from rest. The results are compared with the documented translating case, and a good agreement is found.

The flow field development is first presented for the two cases of Re = 500 and 1000 in the form of streamline patterns. The surface pressure distribution is also presented for a typical case. The time variation of the drag coefficients are first presented for two values of Reynolds number and compared with previously known analytical solutions for the potential flow problem. Comparison between viscous and inviscid flow results show a better agreement for higher values of Re and α. Although numerical results are only obtained for harmonic oscillations, the method of solution presented can be applied to free-stream oscillations of any prescribed form. Moreover, by taking small values of ξ_0, the same method can be used for investigating the interesting case of oscillating viscous flow over a flat plate which may be approximated by a thin elliptic cylinder.

References

Badr, H. M. 1994a Oscillating inviscid flow over elliptic cylinders with flat plates and circular cylinders as special cases. *Ocean Engineering* **21,** 105–113.

Badr, H. M. 1994b Oscillating viscous flow over an inclined elliptic cylinder *Ocean Engineering* **21,** 401–426.

Badr, H. M. & Dennis, S. C. R. 1985 Time-dependent viscous flow past an impulsively started rotating and translating circular cylinder. *Journal of Fluid Mechanics* **158,** 447–488.

Badr, H. M., Dennis, S. C. R., Kocabiyik, S. 1995a Initial oscillatory flow past a circular cylinder, *Journal of Engineering Mathematics* **29,** 255–269.

Badr, H. M., Dennis, S. C. R., Kocabiyik, S. & Nguyen, P. 1995b Viscous oscillatory flow about a circular cylinder at a small to moderate Strouhal number. *Journal of Fluid Mechanics* **303,** 215–232.

Collins, W. M. & Dennis, S. C. R. 1973 Flow past an impulsively started circular cylinder. *Journal of Fluid Mechanics* **60,** 105–127.

Davidson, B. J. & Riley, N. 1972 Jets induced by oscillatory motion. *Journal of Fluid Mechanics* **53,** 287–303.

Honji, H. 1972 Starting flows past spheres and elliptic cylinders. Reports of the Research Institute of Applied Mechanics, Kyushu University, Japan, Vol. XIX, No. 65.

Nguyen, P. & Kocabiyik, S. 1996 On a translating and transversely oscillating cylinder: part 1. Effect of the Strouhal number on the hydrodynamic forces and the near wake structure, *Ocean Engineering* (in press).

Patel, V. A. 1981 Flow around the impulsively started elliptic cylinder at various angles of attack. *Computers and Fluids* **9,** 435–462.

Riley, N. 1967 Oscillatory viscous flows: review and extension. *Journal of Institute of Mathematics and Applications* **3,** 419–436.

Riley, N. & Wybrow, M. F. 1995 The flow induced by the torsional oscillations of an elliptic cylinder. *Journal of Fluid Mechanics* **290,** 279–298.

Staniforth, A. N. 1972 Studies of symmetrical and antisymmetrical viscous flows past impulsively started cylinders. Ph. D. Thesis, The Univeresity of Western Ontario, London, Canada.

Sarpkaya, T. 1979 Vortex-induced oscillations. A selective review. *Journal of Applied Mechanics* **46,** 241–256.

Taneda, S. 1977 Visual study of unsteady separated flows around bodies. *Progress in Aerospace Sciences* **17,** 287–348.

Zhang, J. & Dalton, C. 1993 A numerical comparison of Morison equation coefficients for low Keulegan-Carpenter number flows: both sinusoidal and nonsinusoidal. *Journal of Fluids and Structures* **7,** 39–56.